International Nano Letters
https://doi.org/10.1007/s40089-021-00338-w

ORIGINAL ARTICLE

Facile synthesis and characterization of TiO_2 nanoparticles: X-ray peak profile analysis using Williamson–Hall and Debye–Scherrer methods

S. Mustapha[1,3] · J. O. Tijani[1,3] · M. M. Ndamitso[1,3] · A. S. Abdulkareem[2,3] · D. T. Shuaib[4] · A. T. Amigun[5] · H. L. Abubakar[6]

Received: 4 January 2021 / Accepted: 8 April 2021

Abstract

In this study, TiO_2 nanoparticles were synthesized by a sol–gel method involving the interaction of the titanium isopropoxide precursor and sodium hydroxide followed by calcination at a temperature of 450 °C. The effects of stirring time and solution pH on the morphology, phase types and crystallite sizes were investigated. The prepared TiO_2 nanoparticles were characterized using X-ray diffraction analysis (XRD), high resolution scanning electron microscopy (HRSEM), high-resolution transmission electron microscopy (HRTEM), selective area electron diffraction (SAED), X-ray photoelectron spectroscopy (XPS) and Fourier transform infrared spectroscopy (FTIR). The HRSEM/HRTEM micrograph showed the formation of well distinct TiO_2 nanoparticles with spherical shapes except at pH 2. FTIR spectroscopy showed the presence of the Ti–O stretching modes and Ti–O–Ti vibration modes in the samples. Crystallite size and lattice strain at peak broadening of TiO_2 nanoparticles were studied using Williamson–Hall analysis and Scherrer's equation. It was found that W–H crystallite sizes were significantly different from the sizes obtained from Scherrer's equation at basic medium (pH 8–12) under the applied conditions of stirring time and solution pH for TiO_2 nanoparticles. XRD pattern demonstrated the formation of pure anatase phase of TiO_2 irrespective of the solution pH and stirring time. XPS analysis showed the existence of the Ti 2p orbital in the oxidation states of +4. The study demonstrated that stirring time and solution pH determined the crystallite sizes and not the phase types.

✉ S. Mustapha
saheedmustapha09@gmail.com

[1] Department of Chemistry, Federal University of Technology, PMB 65, Bosso Campus, Minna, Nigeria

[2] Department of Chemical Engineering, Federal University of Technology, PMB 65, Gidan Kwano Campus, Minna, Niger State, Nigeria

[3] Nanotechnology Research Group, Center for Genetic Engineering and Biotechnology, Federal University of Technology, PMB 65, Minna, Niger State, Nigeria

[4] Department of Chemistry, Illinois Institute of Technology, 3101 S Dearborn Street, Chicago, IL 60616, USA

[5] Department of Chemical and Geological Sciences, Al-Hikmah University, Ilorin, Nigeria

[6] Department of Chemistry, Nile University of Nigeria, Airport Road, Jabi, Abuja, Nigeria

Published online: 27 April 2021

Graphic abstract

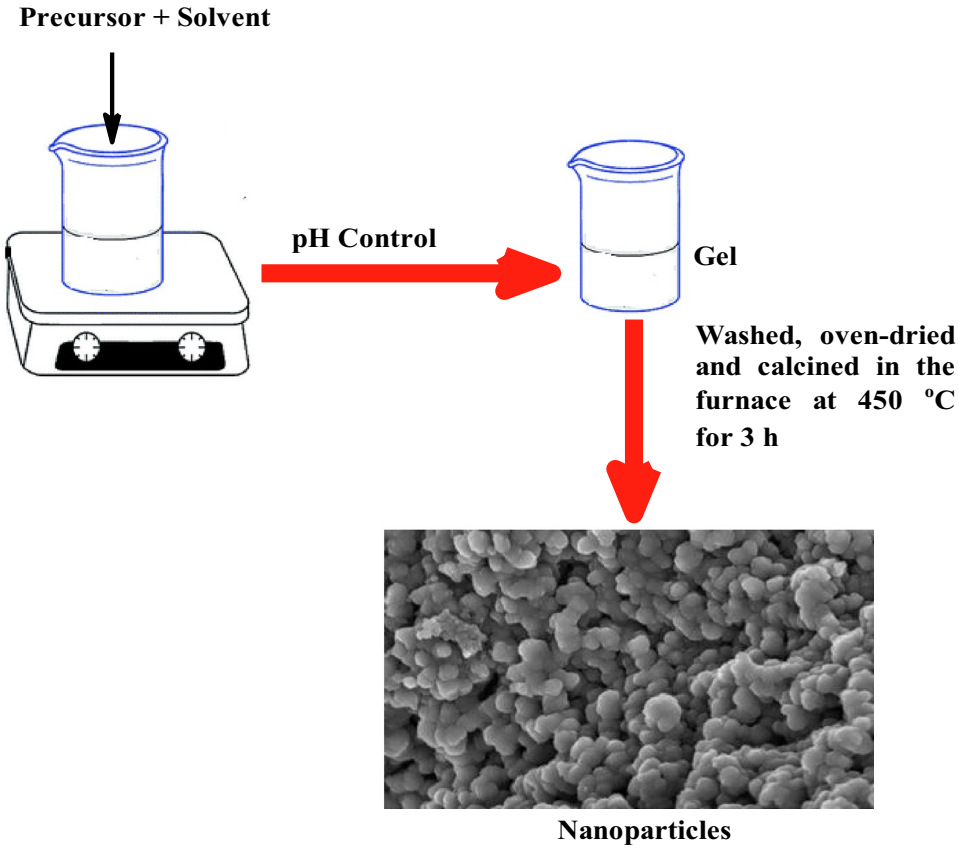

Keywords TiO_2 nanoparticles · Williamson–Hall · Debye Scherrer · Crystalline size · Reflection peaks

Introduction

Researchers in different fields of science and engineering have shown immense interest in nanomaterials due to their electrical, optical, antibacterial, absorptivity, photocatalytic, gas sensitivity, magnetic, chemical and mechanical properties [1–6]. Though, many studies on various types of semiconductors such as titania (TiO_2) [7], MgO [8], Mn_3O_4 [9], ZnO [10–13] and CdS [14] at the nanoscale have been widely documented and practically employed for technological purposes. Particle size and crystal morphology play important roles in these applications, which have motivated researchers on the synthesis of nanocrystalline TiO_2. TiO_2 is a non-toxic n-type semiconductor which exists in the three polymorphs of TiO_2 namely; anatase (tetragonal), rutile (tetragonal) and brookite (orthorhombic). Among these, anatase is considered as a metastable phase at a lower temperature, difficult to prepare due to susceptibility to phase transformation and it possesses excellent chemical and physical properties due to its bandgap energy of 3.2 eV [15]. TiO_2 nanoparticles are considered one of the most beneficial functional materials owing to its excellent optoelectronic properties: sufficient photoreactive properties, high dielectric constant, high transmission coefficient, and high breakdown strength [16].

TiO_2 nanoparticles have been synthesized using various methods which include hydrothermal [17], co-precipitation [18], chemical vapour deposition [19], sol–gel [16], laser ablation [20], spray pyrolysis [21], vacuum arc deposition [22] amongst others. In most studies, precursors such as Titanium isopropoxide, titanium hydroxide, titanium-n-butoxide, titanium tetrachloride, titanium trichloride, titanium sulphate to mention but a few. It is noteworthy to mention that, TiO_2 nanoparticles prepared via conventional gas-phase techniques required the use of sophisticated equipment. These techniques such as physical vapour deposition, spray pyrolysis and sputtering methods caused agglomeration of the particles, requiring complex chemical procedures for the dispersion of nanoparticles in a solvent, thus resulting in poor characteristics and performance. Also, some of these methods required expensive toxic chemicals, high amount of energy and in most cases generate toxic byproducts which

are environmentally friendly. Owing to the disadvantages of these processes, the sol–gel method has been considered as the most suitable route for the synthesis of TiO_2 nanoparticles of controlled size and desired morphology due to its low cost, ease of set-up and reaction temperature. Sol–gel involves the formation of a colloidal suspension through hydrolyzation, polymerization, evaporation and condensation of metal salt precursor. Different researchers have applied the sol–gel method to prepare TiO_2 nanoparticles [23, 24]. They found that synthesis parameters such as solution pH, the concentration of the metal salt precursor, the nature of the metal salt precursor, stirring speed, reaction time, reaction temperature, solution pH influence the shape, size, purity, porosity, surface area and phase types of the metal nanoparticles. These properties which also include crystallinity play a vital role in their applications.

For instance, the pH of the medium significantly affects crystal structure and surface morphology such as the size and the entanglement of TiO_2 nanostructures [25–27]. Tsega and Dejene [28] reported that the morphology and crystallinity of TiO_2 depend on the pH of the precursor solution. Lower acidity promoted the formation of the anatase phase of TiO_2 nanoparticles and greater crystallite size. This shows that the degree of crystallinity of TiO_2 nanoparticles is pH-dependent. However, the possibility of the different phase structure of TiO_2 nanoparticles of different pH solution and the relationship between solution pH and phase types of TiO_2 has not been clearly understood. Not only that, but a detailed study on a crystalline size determination using Williamson–Hall (W–H) analysis and Debye–Scherrer's equation on the TiO_2 nanoparticles synthesized at different pH and stirring time also has not been reported. Therefore, investigation of TiO_2 nanoparticles synthesized under acidic and basic medium is necessary for the clarification of the crystal forms, micro/nanostructure, phase types and optical properties of TiO_2 nanoparticles.

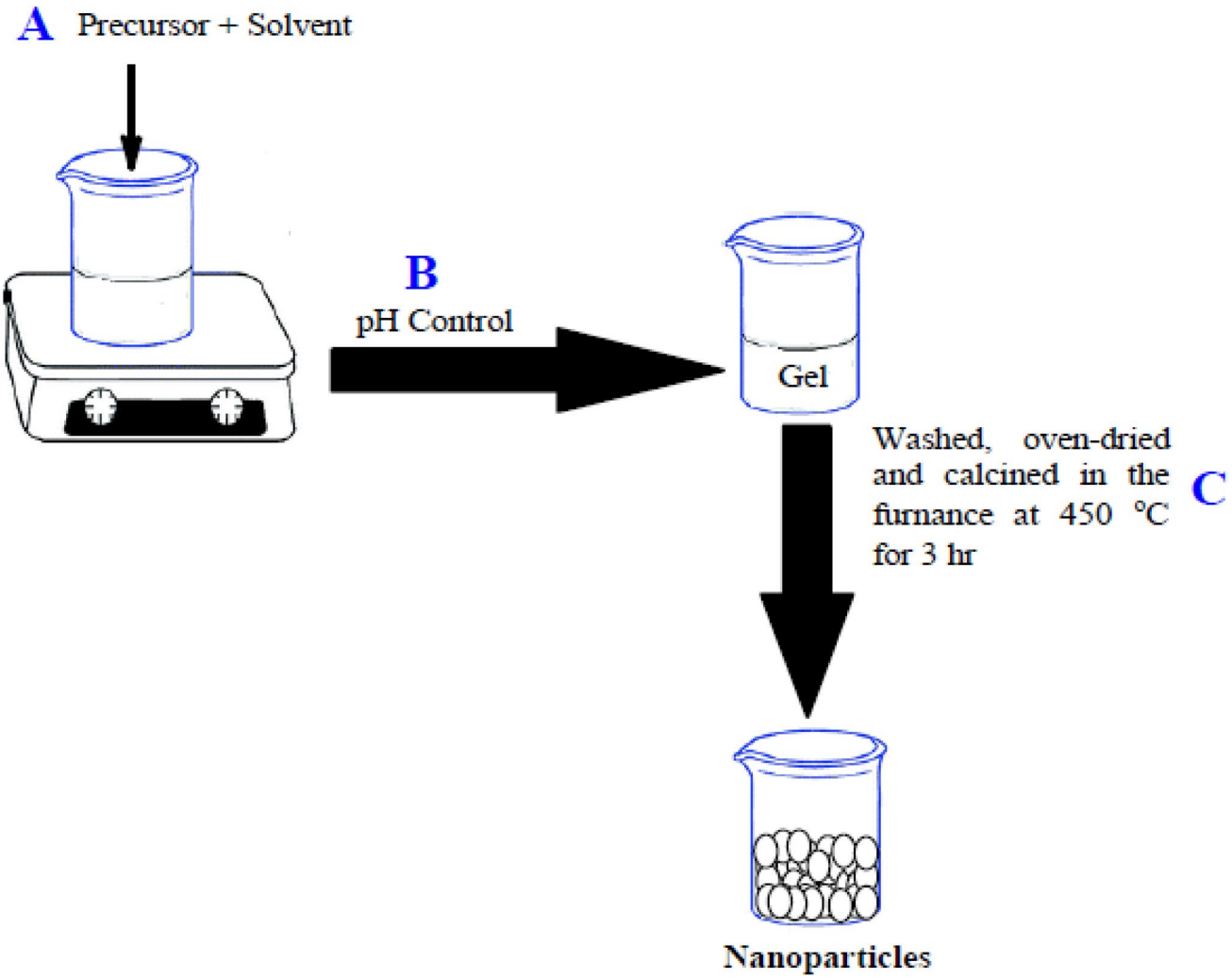

Fig. 1 Pictorial representation of the steps involved in the preparation of TiO_2 nanoparticles using the sol–gel technique

XRD has been a powerful technique in determining the crystal structure, crystalline phases, crystalline orientation, lattice parameters, strain, energy density and among others [29]. X-ray peak profile analysis (XPPA) is a method used to estimate the crystallite size and lattice strain extracted from the peak width analysis. Crystallite size quantifies the size of the coherent diffraction domain while lattice strain measures the distribution of lattice constants arising from lattice dislocation. In previous studies, crystallite sizes on peak broadening of TiO_2 nanoparticles were determined by Priyanka et al. [30]. In their study, the crystallite size obtained using Williamson–Hall and Scherrer Debye equations were performed only for TiO_2 nanoparticles prepared at pH 2 while Kibasomba et al. [31] calculated the crystallite sizes of TiO_2 calcined at the temperature range of 350–650 °C using Williamson–Hall plot method. Also in the studies of Sabry et al. [2], Singh et al. [32], Singh et al. [33] and Fu et al. [34], both Scherrer and Williamson–Hall equations were utilized on TiO_2 nanoparticles calcined at different temperatures. From these studies, it was observed that crystalline sizes for both methods increase with temperature. It can be seen that previous studies focused on the effect of calcination temperatures on the phase types of TiO_2 nanoparticles. In contrast, the present work describes the synthesis of TiO_2 nanoparticles from titanium isopropoxide (TTIP) at a different stirring time and solution pH by the sol–gel method. The morphological, microstructural, functionality and chemical oxidation properties of TiO_2 nanoparticles were investigated by X-ray diffraction, high resolution scanning electron microscope (HRSEM), high-resolution transmission electron microscopy (HRTEM), selected area of electron diffraction (SAED), X-ray photoelectron spectroscopy (XPS) and Fourier-transform infrared (FTIR) spectroscopy. The XXPA was carried out for estimating the crystallite size, lattice strain and dislocation density of TiO_2 nanoparticles using Williamson–Hall analysis and Scherrer's equation.

Materials and methods

Materials

Titanium tetraisopropoxide, $Ti[OCH(CH_3)]_4$, (TTIP, 97%), sodium hydroxide (NaOH, ≥ 97%) and ethanol (C_2H_5OH) (≥ 99.5%) were procured from Sigma Aldrich; and were used as received without further purification. All the reagents were analytical grade chemicals and deionized water was used throughout the study.

Titanium oxide nanoparticle (sol–gel method)

The sol–gel method which involves the variation of stirring time and solution pH was used for the synthesis of TiO_2 nanoparticles and are described as follows:

Effect of stirring time

The steps involved in the effect of stirring times on the synthesis of TiO_2 nanoparticles via sol–gel method follow Fig. 1 without (Step **B**). Five different solutions were prepared as follows: 30 cm^3 of TTIP solution was measured individually into five separate 250 cm^3 beaker containing 120 cm^3 of de-ionized water (Step **A**). The five separate solutions were stirred for 20, 40, 60, 80 and 100 min, respectively, using a magnetic stirrer at 250 rpm. A gel was formed in each of the five solutions at pH 5.62 and washed with de-ionized water and ethanol several times and thereafter, oven-dried at 105 °C for 24 h (Step **C**). The obtained yellow xerogel was pulverized in a mortar to a fine powder and further calcined in the furnace at 450 °C for 3 h (Step **C**).

Effect of pH solution

Figure 1 shows the pictorial representation of the synthesis protocol of TiO_2 nanoparticles via sol–gel method. Another set of five different solutions were prepared as follows: Firstly, 30 cm^3 of the TTIP solution was measured into five separate 250 cm^3 beaker containing 120 cm^3 of de-ionized water. (Step **A**). To each of the five solutions, the pH of the solution was adjusted to 4, 6, 8, 10 and 12, respectively, using 0.5 M nitric acid or 0.5 M sodium hydroxide, followed by vigorous stirring on a magnetic stirrer at 250 rpm for optimum stirring time (smallest crystallite size) (Step **B**). A gel was formed and were allowed to age for 2 h, later washed with de-ionized water and ethanol several times and thereafter, oven-dried at 105 °C for 24 h (Step **C**). The obtained yellow xerogel was pulverized in a mortar to a fine powder and further calcined in the furnace at 450 °C for 3 h (Step **C**).

Characterizations of TiO_2 nanoparticles

The phase and the crystal size of the TiO_2 nanoparticles were determined using X-ray diffraction (Bruker AXS D8 Advance, X-ray diffractometer) with CuKα radiation (1.5406 Å) in the diffraction angles range of 10 to 90° and the phase composition of the sample was examined. The morphology and elemental composition of the nanoparticles were investigated using high-resolution scanning electron microscopy (HRSEM) (Zeiss Auriga model) operated with electron high tension at 5.0 kV for imaging. About 0.05 mg powdered sample was placed onto carbon adhesive tape and sputter-coated with Au–Pd via a Quorum T15OT for some

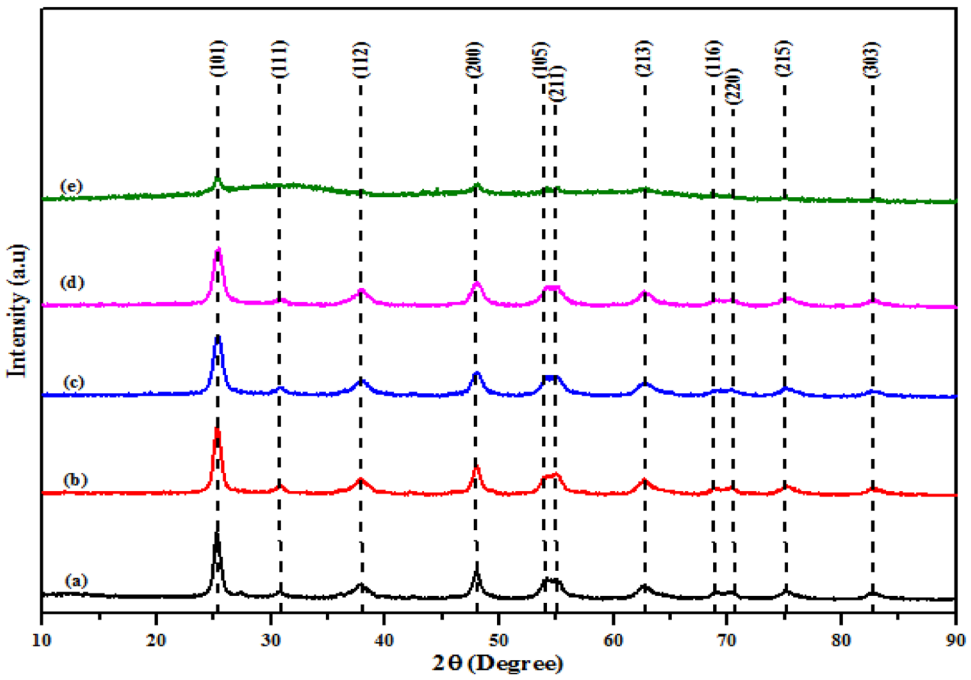

Fig. 2 XRD patterns of TiO_2 nanoparticles produced at different stirring time **a** 20 min **b** 40 min **c** 60 min **d** 80 min and **e** 100 min

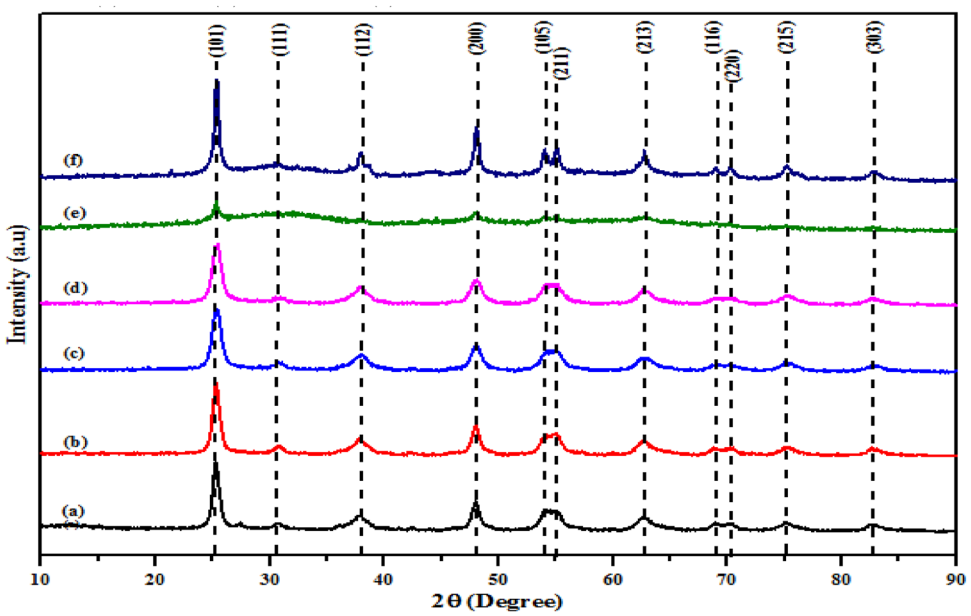

Fig. 3 XRD patterns of TiO_2 nanoparticles produced at different solution pH **a** 2 **b** 4 **c** 6 **d** 8 **e** 10 and **f** 12

minutes before the analysis. The particle size and distribution pattern were analysed by Zeiss Auriga high-resolution transmission electron microscopy (HRTEM) coupled with electron dispersive spectroscopy. The powdered sample (0.02 g) was suspended in 10 cm^3 of methanol, ultrasonicated to achieve total dispersion. Two drops of the slurry were dropped onto a holey carbon grid with the help of a micropipette and then allowed to dry on exposure to a photolight. The Fourier transmission infrared (FTIR) spectra were recorded using the Thermo Scientific Nicolet iS5spectrometer recorded at wavenumber of 4000–500 cm^{-1}. X-ray photoelectrons (XPS) model using a monochromated MgKα (1253.6 eV) at a power of 300 W and 15 eV was used to study the surface composition of the sample.

Table 1 Average crystallite size of TiO_2 at different stirring time for the Scherrer formula and the Williamson–Hall (W–H) analysis

Parameter	Stirring time (min)					
		20	40	60	80	100
Phase		Anatase	Anatase	Anatase	Anatase	Anatase
Scherrer	D (nm)	2.04	3.50	3.63	1.28	3.84
	$\delta(\text{nm})^{-2}\times10^{-1}$	2.40	0.82	0.76	6.10	0.68
Williamson-Hall	D (nm)	5.68	6.03	6.24	5.57	6.46
	$\delta(\text{nm})^{-2}\times10^{-2}$	3.10	2.75	2.57	3.22	2.40
	$\varepsilon\times10^{-1}$	− 0.28	− 0.26	− 0.24	− 0.31	− 0.11
Lattice parameter	a	3.79	3.79	3.79	3.79	3.79
	c	9.51	9.51	9.51	9.51	9.51
	$\frac{c}{a}$	2.51	2.51	2.51	2.51	2.51
Lattice structure		Tetragonal	Tetragonal	Tetragonal	Tetragonal	Tetragonal

Results and discussion

Mechanism of TiO_2 nanoparticles via sol–gel method

The sol–gel method is commonly used to synthesize TiO_2 nanoparticles and the frequent metal and non-metal alkoxides precursors are titanium (IV) tetraisopropoxide (TTIP), titanium chloride, titanium (IV) tert-butoxide, bis (cyclooctatetraene) titanium, tetraisopropylorthotitanate (TIPT), potassium titanium oxalate (KTO), butyl titanate (TBT) and titanium (IV) butoxide [32, 35]. During this process, the colloid is formed after the hydrolysis and polycondensation reactions. An acid and a base help in the hydrolysis of the precursor followed by the growth and agglomeration of particles. This process proceeds by hydrolytic polycondensation of titanium precursors being alkoxides or chlorides in the presence of solvents, modifiers, and organic templates. The reaction starts with hydrolysis, which is the formation of Ti–OH moieties by the substitution reaction of water with Ti-OR groups. The precursors further undergo condensation reactions to produce Ti–O–Ti by oxolation or Ti–OH–Ti bonds by olation [36].

XRD analysis

The XRD patterns of TiO_2 nanoparticles prepared at different stirring times and solution pH are shown in Figs. 2 and 3, respectively. According to different scholars, the production of different of phases of titania depends on calcination temperatures and it has been reported that the formation of anatase occurred at a lower temperature less than 600 °C [37, 38]. This informed the choice of calcination temperature of 450 °C for the production of titania. The choice of calcination temperature was based on the formation of titania with the anatase phase. Figure 2 revealed the presence of several diffraction peaks at 2 theta values of 25.28°, 30.79°, 38.58°, 48.05°, 53.89°, 55.06°, 62.12°, 68.76°, 70.31°, 75.03° and 82.14° which correspond to the following Miller indices (101), (111), (112), (200), (105), (211), (213), (116), (220), (215) and (303), respectively. This information is in harmony with the Joint Committee on Powder Diffraction Standard (JCPDS) No. 00–021-1272 of a typical tetragonal TiO_2 anatase phase irrespective of the stirring time with parameters $a=b=3.79$ Å, $c=9.51$ Å, $\frac{a}{c}=2.51$, cell volume = 136.31 Å, density = 3.89. No trace of brookite or rutile phase was detected as a function of stirring times, and non-detection of these phases suggests high purity of as-synthesized TiO_2 nanoparticles under the applied conditions. The similar tetragonal anatase phase of TiO_2 nanoparticles prepared using the sol–gel method had been reported by Kang et al. [23] and Nateq and Ceccato [24]. It can be seen that the XRD patterns of the TiO_2 nanoparticles were similar with anatase peaks at almost the same diffraction angles as displayed in Fig. 2. This indicates that stirring time did not influence the phase types of TiO_2 nanoparticles but rather crystallite sizes. Crystallite sizes were calculated using Dybe–Scherrer and Williamson–Hall expression shown in Eqs. 1 and 2 and the values obtained were compared:

$$D=\frac{k\lambda}{\beta\cos\theta} \tag{1}$$

where D is the crystallite size (nm), k is a constant (0.94 for spherical particles), λ is the wavelength of the X-ray radiation (CuKα = 0.1541 nm), β is the full width at half maximum (FWHM) of the intense and broad peaks, ε is the lattice strain while θ is the Bragg's or diffraction angle.

$$\beta\cos\theta=\frac{k\lambda}{D}+4\varepsilon\sin\theta \tag{2}$$

Crystalline size obtained using Eq. (1) at stirring time of 20, 40, 60, 80 and 100 min were 2.04, 3.50, 3.63, 1.24 and 3.84 nm (see Table 1). The smallest crystallite size (1.24 nm) was obtained at stirring time of 80 min and

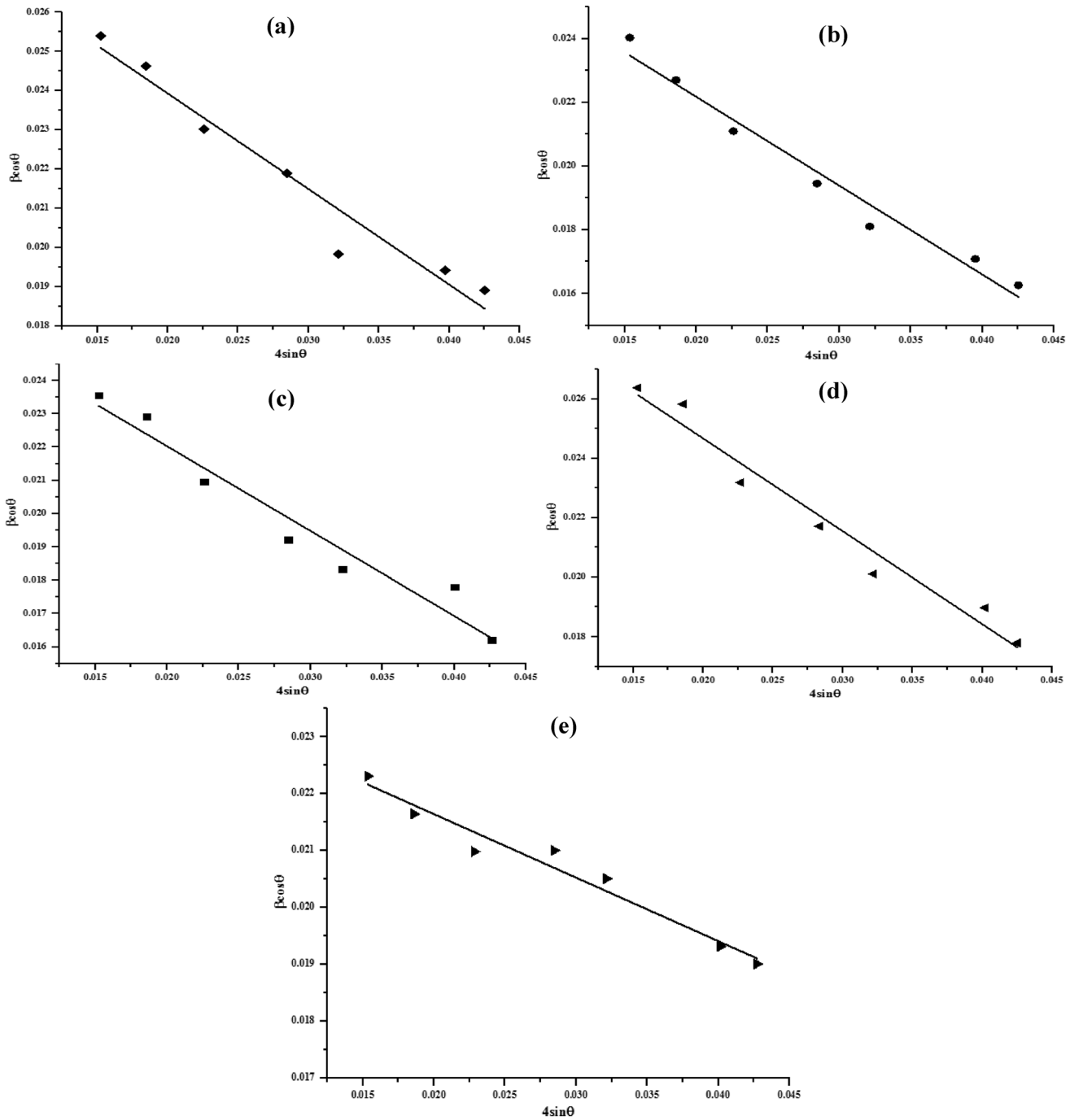

Fig. 4 A Williamson-Hall plot of $\beta\cos\theta$ against $4\sin\theta$ calculated from XRD diffractogram for TiO_2 nanoparticles at stirring time **a** 20 min **b** 40 **c** 60 min **d** 80 and **e** 100 min calcined at 450 °C

therefore selected as the optimum stirring time to synthesize TiO_2 nanoparticles. A slight difference in terms of crystallite size and optimum stirring time when the Williamson–Hall equation was observed while there were significant differences in the crystallite sizes obtained using Williamson–Hall and Dybe-Scherrer equations. The separation of size and lattice strain broadening analysis was done using Williamson–Hall alone. The crystallite size reported in this study was smaller than 22.9 nm reported by Netaq and Ceccato [24] who also employed a sol–gel method based on hydrolysis-condensation of titanium tetraisopropoxide in solutions of water/cyclohexane/Triton X-100 system. The possible reasons for the variation

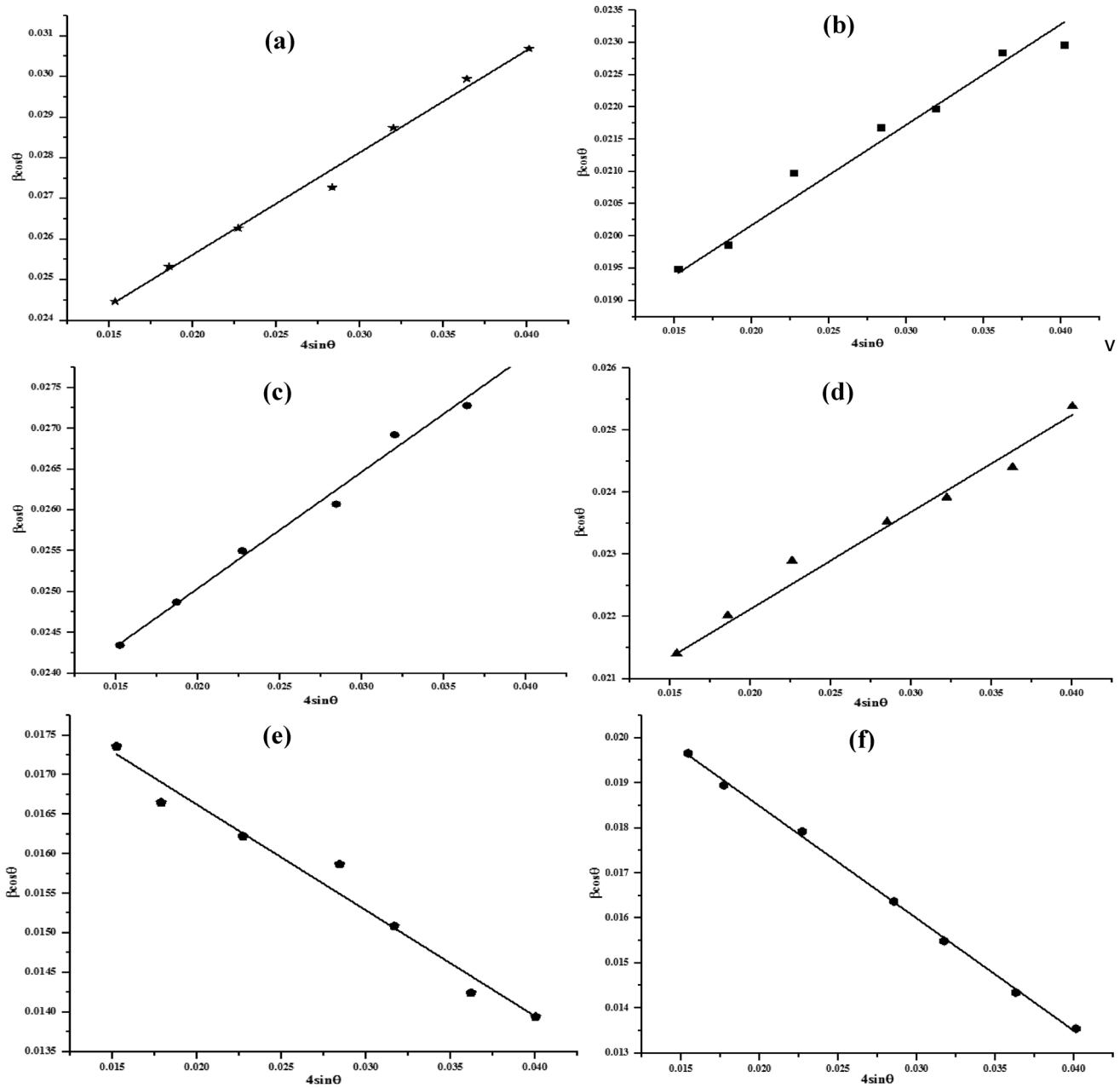

Fig. 5 A Williamson-Hall plot of $\beta\cos\theta$ against $4\sin\theta$ calculated from XRD diffractogram for TiO_2 nanoparticles at pH **a** 2 **b** 4 **c** 6 **d** 8 **e** 10 and **f** 12 calcined at 450 °C

in the crystallite sizes may be ascribed to differences in calcination temperature and solvent types used.

As shown in Fig. 3, it can be seen that the Bragg's peaks were more intense at 2 theta value of 25.28° (101) than other diffraction angles, which suggest the formation of TiO_2 nanoparticles of large crystallite size. While the peaks of low intensity and the broad base became more prominent, indicating the formation of nanoparticles of smaller sizes. The difference in the crystallite sizes at different pH values could be attributed to the amount of H^+ or OH^- during the growth or nucleation of the titanium crystals. At low pH (2) to (6), there was strong electrostatic repulsion between the hydrogen ion and positively charged Ti ion and may be responsible for the small crystallite sizes. This suggests that the acidic medium favours the formation of TiO_2 nanoparticles of small crystallite sizes. While at high pH (10) and (12), there was an occurrence of strong electrostatic attraction between the negatively charged hydroxyl ions and positively charged Ti ion, which eventually result in the formation of $Ti(OH)_4$. Upon the

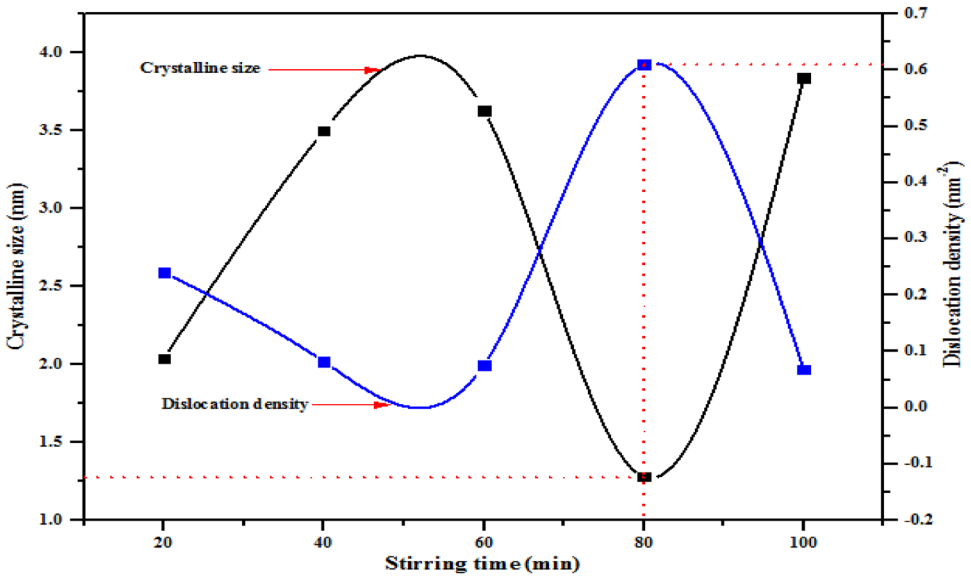

Fig. 6 The plot of crystalline size and dislocation density against stirring time of TiO_2 nanoparticles using Debye–Scherrer analysis

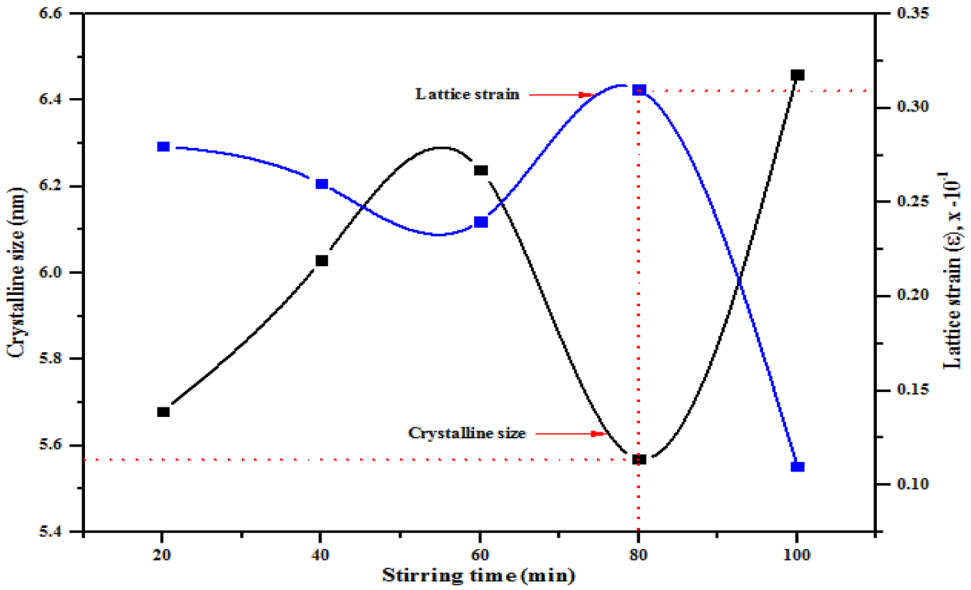

Fig. 7 The plot of crystallite size and lattice strain against stirring time of TiO_2 nanoparticles using Williamson-Hall analysis

calcination of $Ti(OH)_4$ precipitate in the furnace, TiO_2 nanoparticles of larger crystallite sizes were formed. Furthermore, the dislocation density (δ) was calculated using Eq. (3) and the result is shown in Table 1.

$$\delta = \frac{1}{D^2} \tag{3}$$

Scherrer and Williamson–Hall equations were employed in the determination of average crystallite size, dislocation density and lattice strain of the TiO_2 nanoparticles at different stirring times. The plots of $\beta\cos\theta$ against $4\sin\theta$ for the TiO_2 nanoparticles at different stirring times and pH values give straight lines as shown in Fig. 4 and 5, respectively. The respective values of lattice strain and average crystalline size were calculated from the slope and intercept. The plots of W–H for TiO_2 nanoparticles (from Fig. 4) gave grain sizes of the stirring times that are slightly more than the results obtained from Scherrer's equation. Thus, indicating that Scherrer's equation employed for average particle size determination fitted well for the TiO_2 nanoparticles.

The dislocation density is inversely proportional to the grain size/crystallite size of TiO_2 nanoparticles calculated using Debye Scherrer's formula. According to Table 1, it was noticed that the dislocation density decreased with increase in stirring times from 20 to 60 min and beyond this time, the sudden increase was observed precisely at 80 min and the increment was due to the reduction and rearrangement in the

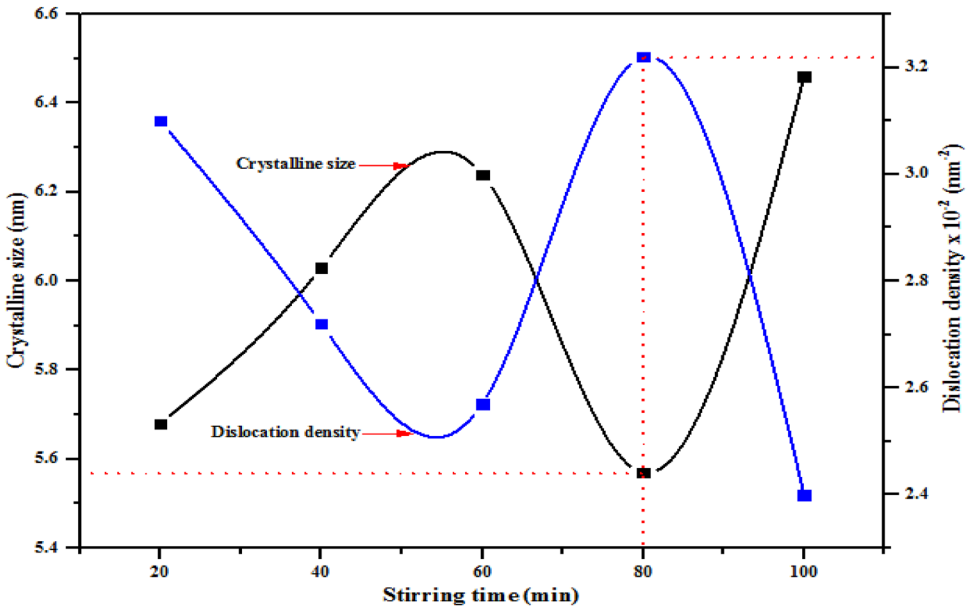

Fig. 8 The plot of crystalline size and dislocation density against stirring time of TiO_2 nanoparticles using Williamson-Hall analysis

Table 2 Average crystallite size of TiO_2 at different pH for the Scherrer formula and the Williamson–Hall (W–H) analysis

Parameter		pH					
		2	4	6	8	10	12
Phase		Anatase	Anatase	Anatase	Anatase	Anatase	Anatase
Scherrer	D (nm)	2.24	1.96	1.85	1.52	3.90	4.74
	$\delta(\text{nm})^{-2}\times10^{-1}$	1.99	2.60	2.92	4.33	0.66	0.45
Williamson-Hall	D (nm)	5.98	6.08	6.89	7.62	7.32	8.25
	$\delta(\text{nm}^{-2})\times10^{-2}$	2.80	2.71	2.11	1.72	1.87	1.47
	$\varepsilon\times10^{-1}$	2.51	1.62	1.43	1.56	− 1.34	-2.49
Lattice parameter	a	3.79	3.79	3.79	3.79	3.79	3.79
	c	9.51	9.51	9.51	9.51	9.51	9.51
	$\frac{c}{a}$	2.51	2.51	2.51	2.51	2.51	2.51
Lattice structure		Tetragonal	Tetragonal	Tetragonal	Tetragonal	Tetragonal	Tetragonal

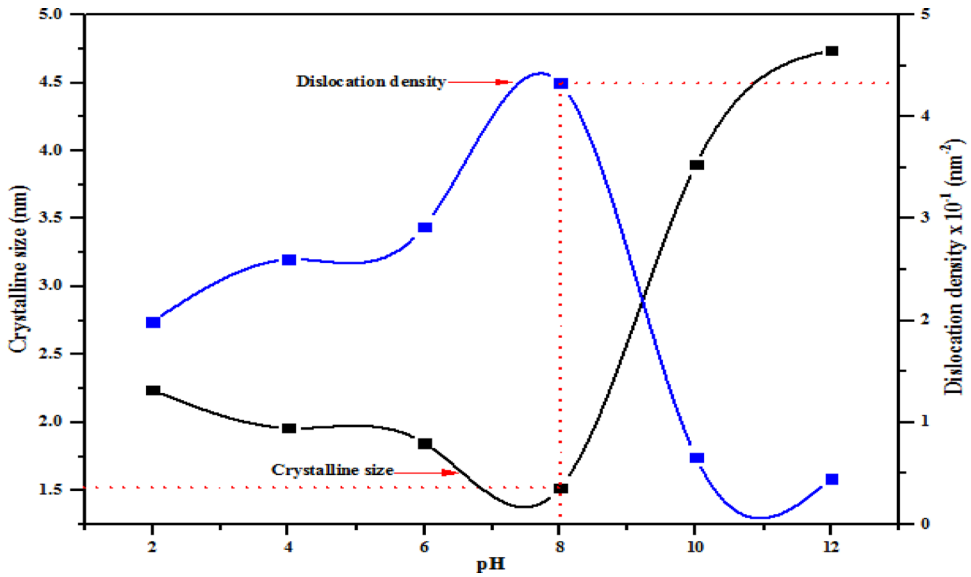

Fig. 9 The plot of crystalline size and dislocation density against pH of TiO_2 nanoparticles using Dybe-Scherrer analysis

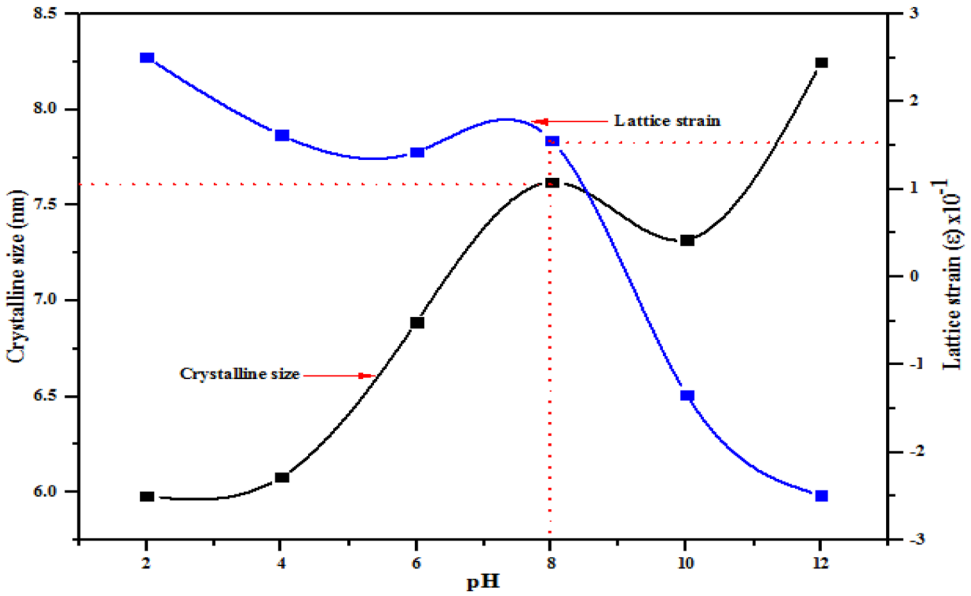

Fig. 10 The plot of crystallite size and lattice strain against pH of TiO_2 nanoparticles using Williamson-Hall analysis

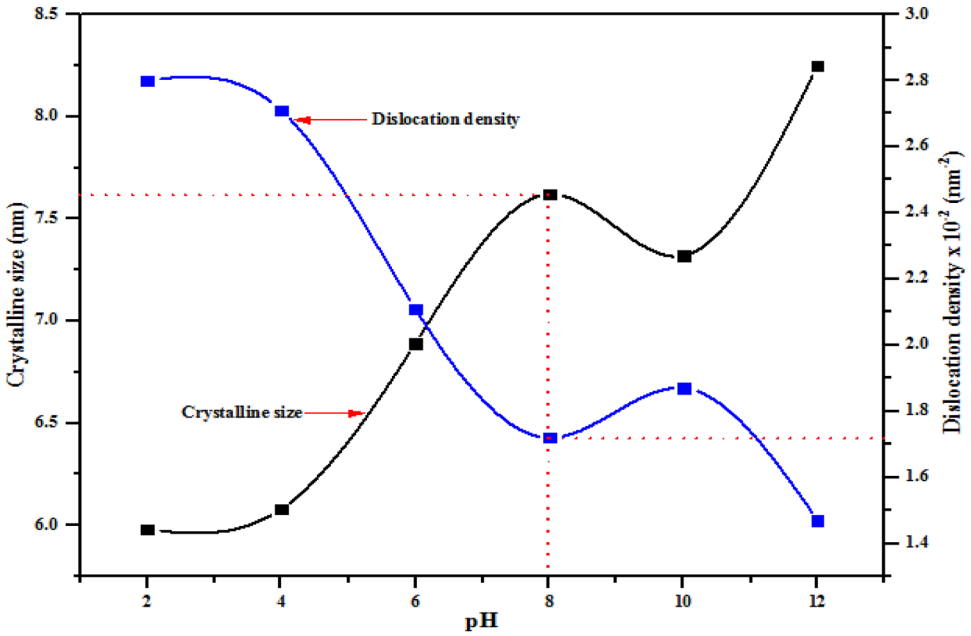

Fig. 11 The plot of crystalline size and dislocation density against pH of TiO_2 using Williamson-Hall analysis

crystallite size of TiO_2. The plots of crystalline size, dislocation density and lattice strain versus stirring time using Scherrer and Williamson–Hall analysis are shown in Figs. 6, 7 and 8. The highest dislocation density was obtained at 80 min, which is an indication of inverse proportionality of both parameters as described in Figs. 6 and 8. The relationships between FWHM and lattice strain, ε according to the Williamson–Hall equation were calculated and presented in Tables 1 and 2.

As presented in Table 2, Scherrer and Williamson–Hall equations were employed in the evaluation of average crystallite size, dislocation density and lattice strain of the TiO_2 nanoparticles prepared via variation of solution pH. As observed in Table 2, the change in pH (either acidic or basic medium) did not cause phase transformation of TiO_2 nanoparticles from anatase to rutile or anatase to brookite instead variations in crystallite sizes were observed. This showed that an acidic or basic medium (oxolation and deoxolation occur) and further condensation led to the formation of pure anatase phase [39, 40]. This study strongly proved that the mechanism of formation of the crystalline structure via adjustment of the pH only affect the crystallite size and not necessarily the phase types formed. Similar to what was observed earlier under the variation of stirring times, strong

Table 3 Comparison of calculated crystallite sizes using Debye–Scherrer and Williamson–Hall equations from the previous studies and the present study

Crystallite size (nm)	Scherrer	Williamson–Hall	JCPDS No	Crystal structure	Position (2 θ)	Miller indices	References
18.05	36.78		Anatase, 00-004-0477	Tetragonal	25.12°, 37.72°, 47.92°, 53.88°, 54.88°, 62.61°	Not listed	Bitaraf et al. [44]
36.966	49.575		Anatase, 21-1272 and Rutile, 17-0923	Tetragonal	25.32°, 36.99°, 48.07°, 54.38°, 62.65°	(101), (103), (200), (105), (213)	El-Nagar et al. [45]
8.03	–		Anatase, 84-1286 and Rutile, 86-0147	Tetragonal	Not listed	**A**: (101), (103), (200), (105), (204), (116), (215) **R**: (110)	Raguram and Rajiu [46]
11–31	–		JCPDS-ICDD	Not mentioned	**A**: 25.32°, 36.988°, 27.852°, 38.603°, 48.049°, 53.949°, 55.048°, 62.663°, 68.901°, 70.225°, 75.144°, 82.743° **R**: 27.447°, 36.086°, 41.273°, 54.365°, 76.349°	**A**: (101), (103), (004), (112), (200), (105), (211), (204), (116), (220), (215), (224) **R**: (110), (101), (111), (211), (202)	Rajan and Hassan [47]
12.3	–		Anatase, 21-1272	Not mentioned	25°, 38°, 48°, 54°	(101), (004), (200), (105)	Gao et al. [48]
26	–		Anatase, 21-1272	Not mentioned	25.8°, 36.9°, 38.5°, 48.0°, 53.8°, 55.0°, 62.8°, 68.7°, 70.3°	(101), (103), (004), (112), (200), (105), (211), (204), (116), (220)	Ibrahim et al. [49]
9.64	–		Anatase, 89-4921	Tetragonal	Not listed	(101), (004), (200), (105), (211), (204), (116), (220), (107)	Komaraiah et al. [50]
70.1	–		Anatase, 01-073-1764	Tetragonal	Not listed	(101), (103), (004), (112), (200), (105), (211), (203), (220), (107), (215)	Nabi et al. [51]
7.29	–		Anatase, 21-1272	Not mentioned	25.28°, 36.95°, 48.05°, 55.06°, 62.69°, 70.91°	(101), (004), (200), (211), (204), (116)	Ndabankulu et al. [52]
50	–		Anatase, 21-1272	Not mentioned	7.36°, 10.31°, 12.66°, 21.90°, 24.21°, 27.32°, 30.14°, 30.19°, 34.41°	(200), (220), (222), (440), (531), (620), (644), (660), (662)	Azizi-Lalabadi et al. [53]
–			Anatase, 01-086-1157	Not mentioned	25.31°, 37.81°, 48.08°, 54.06°, 62.94°, 69.04°, 75.30°	(101), (004), (200), (105), (211), (220), (215)	Siliveri et al. [54]
20	–		Anatase, 21-1272	Tetragonal	25°, 38°, 48°, 53°, 55°, 62°, 68°, 70°, 75°	(101), (004), (200), (105), (211), (213), (116), (220), (215)	Venkatachalam et al. [55]
10	–		Anatase, 21-1272	Tetragonal	25.3°, 37.8°, 48.1°, 53.9°, 55.1°, 62.7°	(101), (004), (200), (105), (211), (204)	Wu et al. [56]
2.04–4.74	5.57–8.25		Anatase, 00-21-1272	Tetragonal	25.28°, 30.79°, 38.58°, 48.05°, 53.89°, 55.06°, 62.12°, 68.76°, 70.31°, 75.03°, 82.14°	(101), (111), (112), (200), (105), (211), (213), (116), (220), (215), (303)	Present study

A Anatase and *R* Rutile

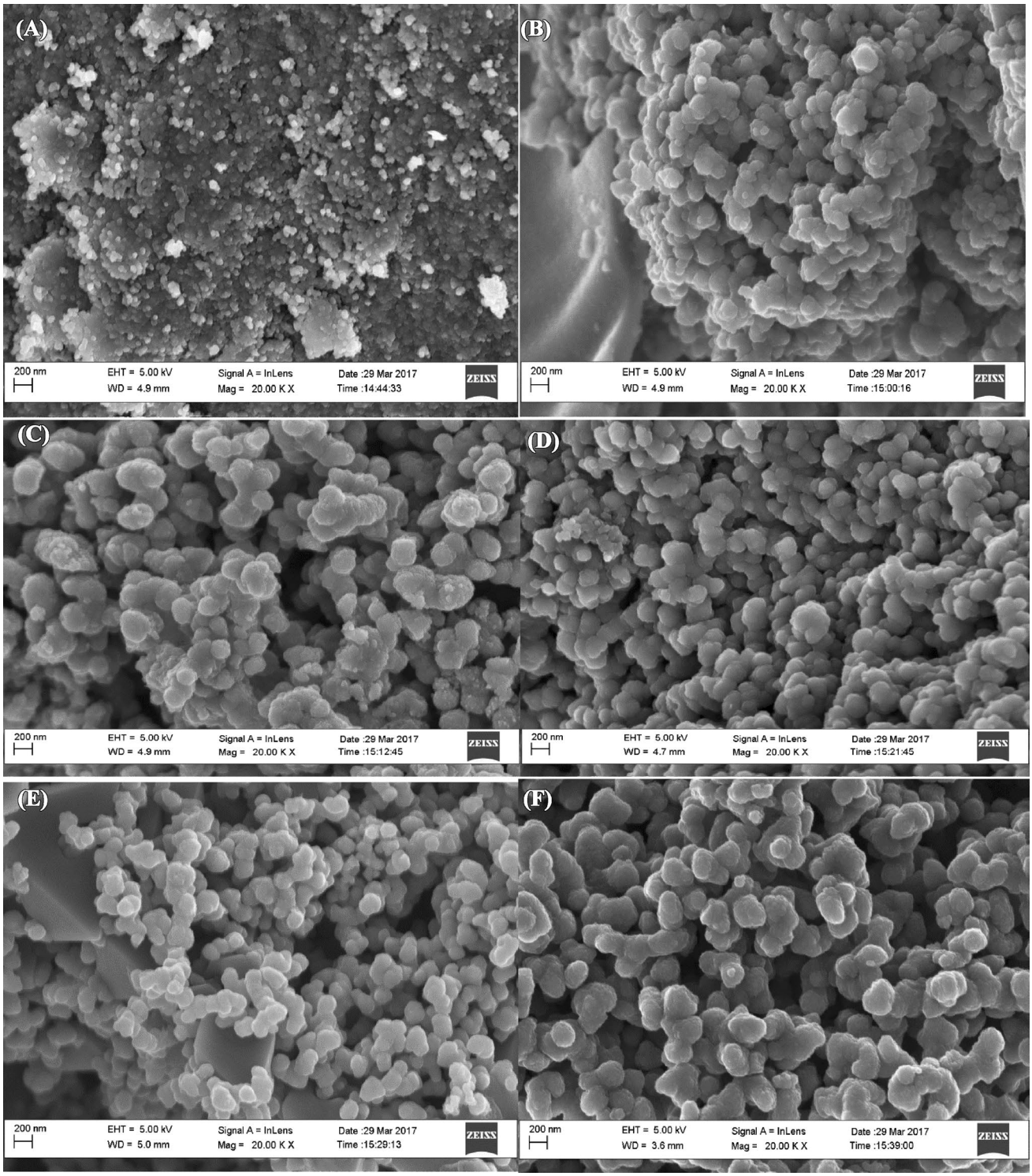

Fig. 12 SEM Analysis of TiO_2 nanoparticles at different pH **a** 2 **b** 4 **c** 6 **d** 8 **e** 10 and **f** 12 calcined at 450 °C

and intense diffraction peaks which correspond to a typical anatase phase of TiO_2 nanoparticles were repeated irrespective of solution pH. Again, TiO_2 nanoparticles with the smallest crystallite size of 1.52 nm were formed at the basic medium (pH 8). Comparatively, it was found that the pH of the medium exhibited a significant effect on the crystallite sizes of TiO_2 nanoparticles than the stirring time due to the smaller crystallite sizes obtained from the former than the latter. The sharp and intense diffraction peaks observed at

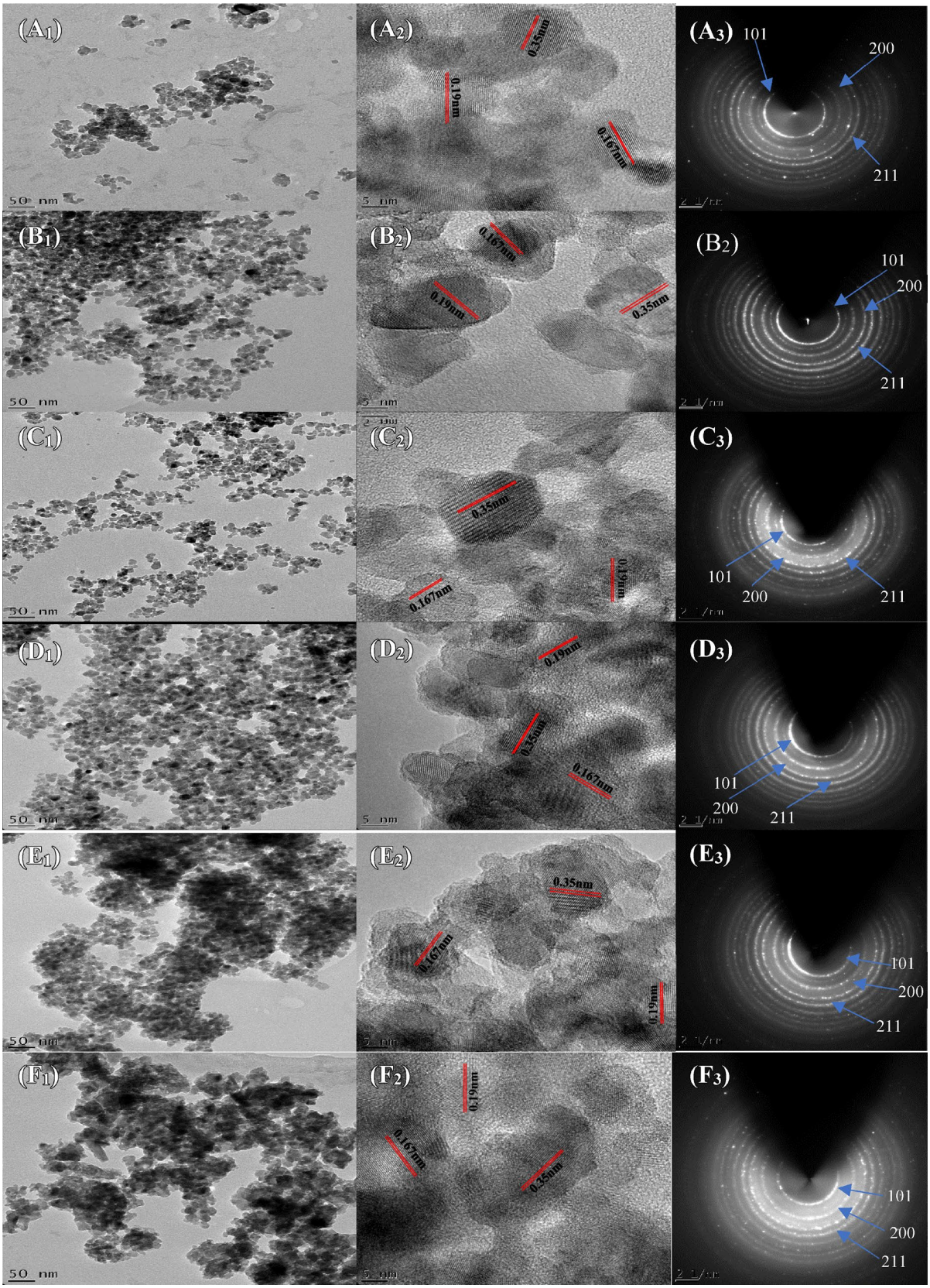

Fig. 13 HRTEM and SAED images of TiO_2 at pH **a** 2 **b** 4 **c** 6 **d** 8 **e** 10 and **f** 12

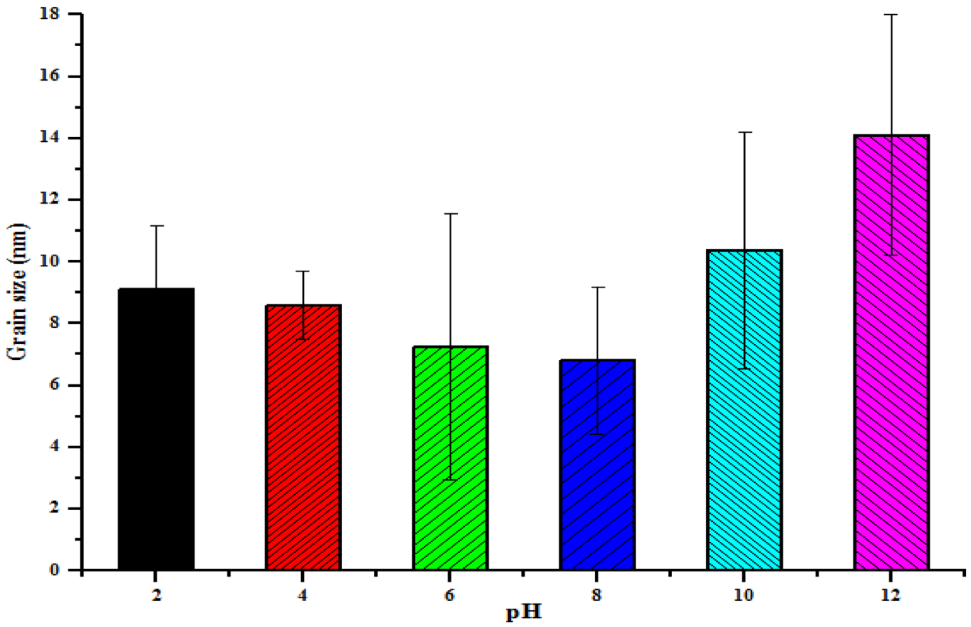

Fig. 14 The plot of grain size against different pH of TiO_2 nanoparticles from HRTEM

pH 12 in the XRD patterns were attributed to the fast nucleation, which increases the crystallinity and average crystallite size of the sample. Thus, this is quite different from the broad diffractograms obtained for lower pH values.

The plots of Williamson–Hall analysis of TiO_2 nanoparticles of different pH as presented in Fig. 5 give the average crystallite size and strain estimated from linear fit data. The results provide coherent values of lattice strain which range from − 0.249 to 0.251. The small values obtained for the lattice parameters could lead to larger surface areas and more active sites [41]. It was observed that with the increase in pH from 2 to 12, the strain associated with the TiO_2 samples decreased, as shown in Table 2 due to the reduction in the level of hydrogen ion in the medium. This effect may be due to the theory of nucleation caused by the crystal growth of nanoparticles [42, 43]. The graphs of crystalline size, dislocation density and lattice strain against pH using Scherrer and William-Hall analysis are shown in Figs. 9, 10 and 11. The lattice strains as presented in Tables 1 and 2 contained positive and negative values. The significant positive and negative values imply compressive and tensile strain. This is attributed to the lattice shrinkage and lattice expansion under the influence of compressive and tensile strain, respectively. The lattice strain numbers at pH 10 and 12 reduce during the growth phase corresponding to their W–H measurements. The negative values of strain are related to compressive strain. Table 3 shows the comparison of calculated crystallite sizes using Debye–Scherrer and Williamson–Hall equations from the previous studies and the present study.

Table 3 shows that the estimated crystallite sizes and the phase types of TiO_2 nanoparticles depend on several factors

Table 4 The average grain size of TiO_2 nanoparticles of HRTEM images

pH	Phase	Average grain size (nm)
2	Anatase	9.11 ± 2.05
4	Anatase	8.60 ± 1.10
6	Anatase	7.24 ± 4.30
8	Anatase	6.80 ± 2.37
10	Anatase	10.36 ± 3.82
12	Anatase	14.10 ± 3.90

such as the method of synthesis, synthesis parameters varied such as solution pH, stirring speed, stirring time, temperature, calcination temperature, holding time, concentration and nature of the salt precursors amongst others. The average crystallite sizes obtained in this study using the two equations differed on tetragonal anatase phase of TiO_2 nanoparticles produced.

HRSEM analysis

HRSEM and HRTEM analysis were only carried out on TiO_2 nanoparticles prepared at different pH. The preliminary XRD results show that stirring time has a significant effect on the sizes and shapes of TiO_2 nanoparticles. The surface morphologies of the synthesized TiO_2 nanoparticles at different pH (a) 2 (b) 4 (c) 6 (d) 8 (e) 10 (f) 12 were shown in Fig. 12. These micrographs displayed that the size of the particles was influenced by the experimental pH condition, indicating randomly and cluster distribution

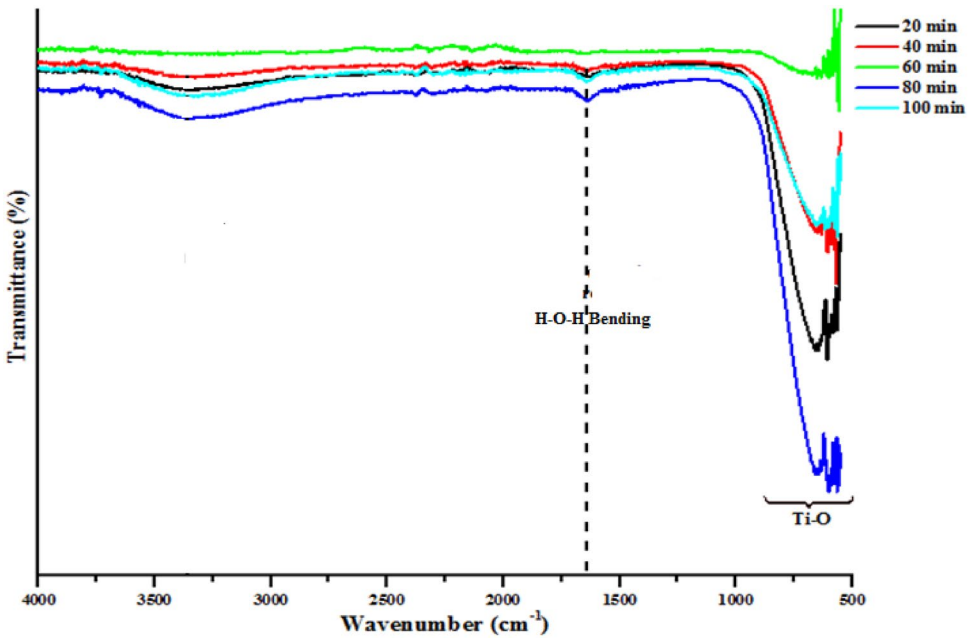

Fig. 15 FTIR of the TIO_2 at stirring time of **a** 20 min **b** 40 min **c** 60 min **d** 80 min and **e** 100 min

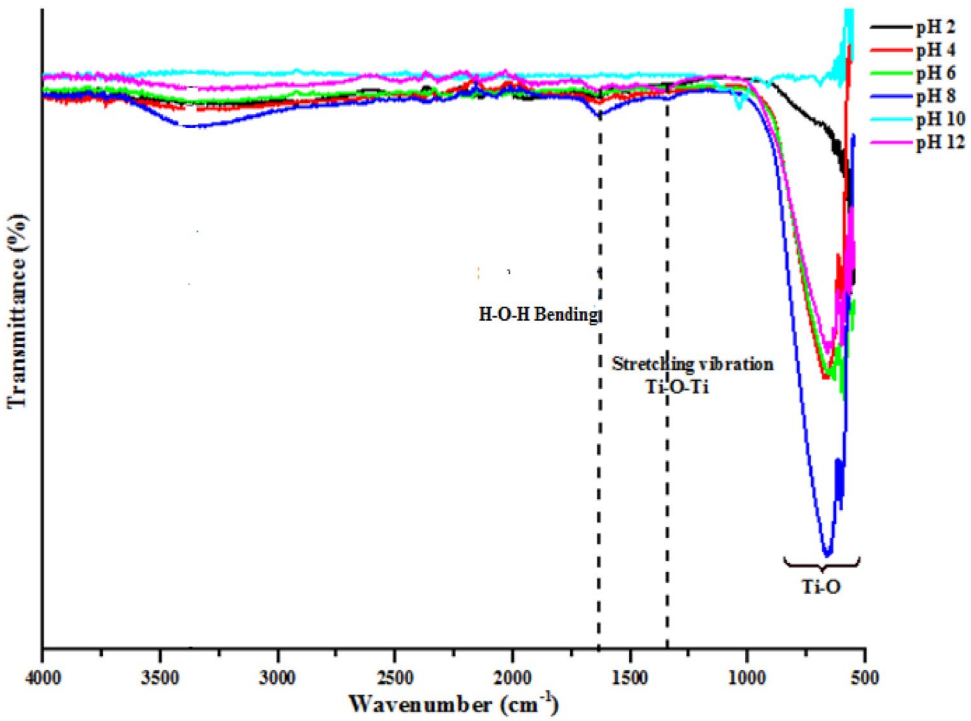

Fig. 16 The FTIR spectra of TiO_2 nanoparticles at pH **a** 2 **b** 4 **c** 6 **d** 8 **e** 10 and **f** 12 calcined at 450 °C

of spherical TiO_2 nanoparticles except at pH (2). At acidic medium, the concentration of hydrogen ions overshadows that of the positively charged Ti ion thus resulted in electrostatic repulsion and partial formation of TiO_2 nanoparticles. With an increase in pH from 8 to 12, the concentration of hydroxyl ion exceeds that of hydrogen ions, and thus electrostatic attractions occurred leading to the formation of agglomerated spherical particles. At higher pH values, deoxolation due to condensation took place (at this point, the amount of hydroxyl ions in the solution was greater than the positively charged Ti ion leading to the formation of well-defined and evenly distributed spherical-shaped material [57]. Therefore, the nano-crystalline structure produced was pH-dependent and promoted the yield of anatase phase

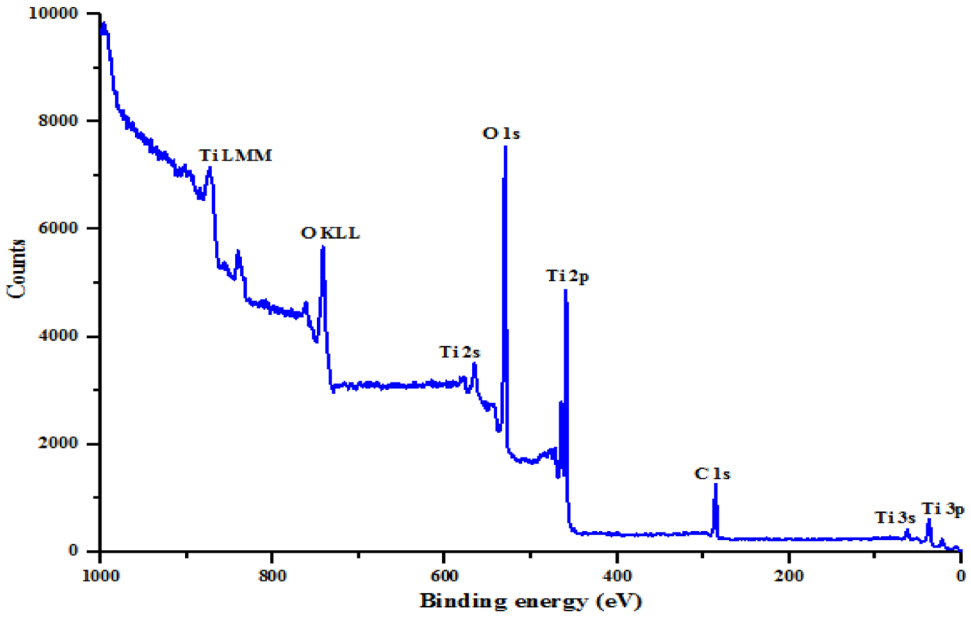

Fig. 17 General XPS survey spectra of TiO_2 nanoparticles

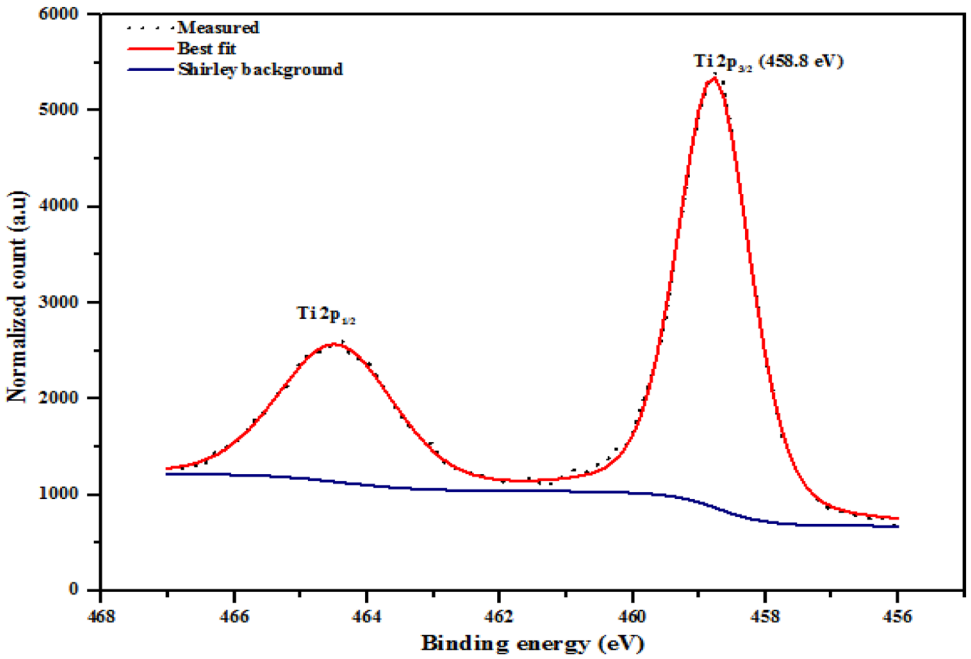

Fig. 18 XPS high-resolution spectrum; Ti 2p spectra of anatase TiO_2 nanoparticles

of TiO_2. The reaction mechanisms for the formation of TiO_2 nanoparticles at lower and higher pH conditions in Eqs. (4) and (5) are as follows:

$$\text{Acidic condition}: \ TiO_2 + nH^+ \rightarrow TiO_2H_n^{+n} \tag{4}$$

$$\text{Basic condition}: \ TiO_2 + nOH^- \rightarrow TiO_2(OH)_n^{-n} \tag{5}$$

With the increasing pH values in the sol–gel method, the TiO_2 samples possess well-defined shape (spherical) and particle sizes, which are as a result of a precipitating agent (NaOH). This showed that the precipitating agent used in this study completely controlled and improved dispersivity. As shown in the HRSEM images (Fig. 13 c, d, e and f), presence of voids or spaces in between the particles suggests the occurrence of inter-particle porosity. Generally, the spheroidal well-dispersed homogeneous and spherical crystal morphologies of TiO_2 samples were more evident in the basic medium than the acidic medium.

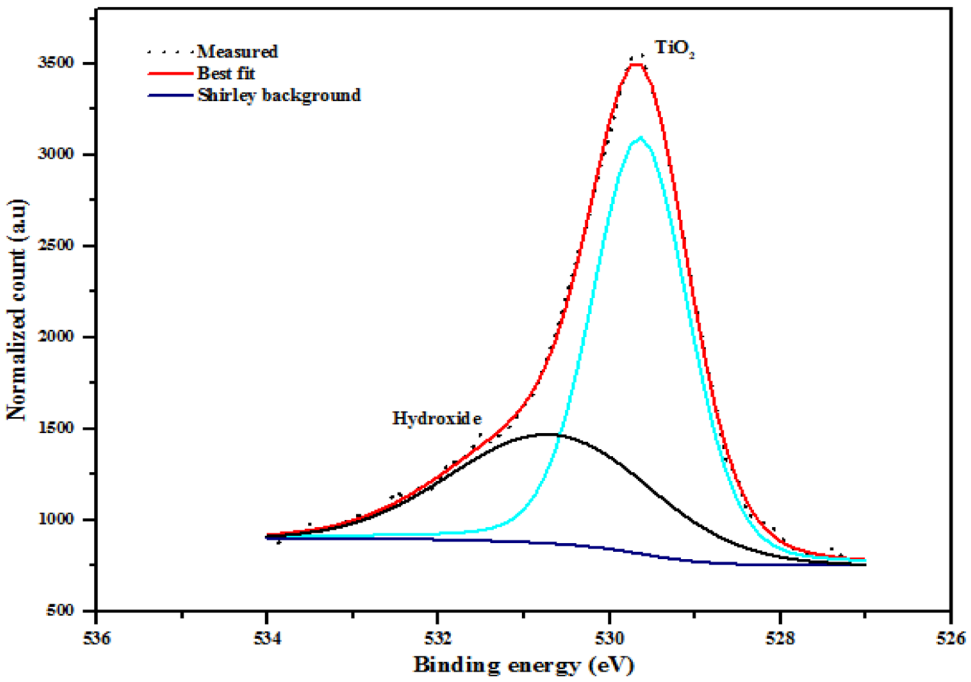

Fig. 19 XPS high-resolution spectrum; O 1 s spectra of anatase TiO_2 nanoparticles

HRTEM analysis

Figure 14 shows the HRTEM images of TiO_2 nanoparticles prepared at different pH (a) 2 (b) 4 (c) 6 (d) 8 (e) 10 and (f) 12. It was shown that the samples consist of spherical crystalline sizes of TiO_2 nanoparticles with the average particle size range from 6.80 to 14.10 nm. Lattice fringes observed in HRTEM is evidence of the formation of well-crystallized TiO_2 material under the applied conditions. HRTEM micrograph also showed the d-spacing of TiO_2 planes which correspond to the results obtained from XRD and SAED patterns. The spectrum recorded for elemental composition of TiO_2 nanoparticles gave well-defined peaks related to tea, O, C, and Ni for the as-synthesized TiO_2 at acidic medium, but Na was found in the as-synthesized TiO_2 at pH > 7. The presence of oxygen was linked to the interaction of the precursor with air during synthesis (washing with ethanol and water) or during calcination in the furnace under air atmosphere. This indicates that the non-metal is in stoichiometric amount with another element present; leading to better performance of adsorption activity. The black spot observed on the HRTEM image patterns at pH 10 and 12 could be attributed to overlaying TiO_2 particles, while the C was from the carbon support film on the TEM grid. According to Fig. 14, the inter-planar distance between lattice fringes of 0.35, 0.19 and 0.16 nm confirmed the (101), (200) and (211) planes of anatase TiO_2 structure, respectively. The SAED patterns of the well-crystallized TiO_2 nanoparticles exhibit diffraction concentric ring pattern, corresponding to a polycrystalline anatase phase. Table 4 shows the grain sizes of HRTEM images of TiO_2 nanoparticles and the plotted graph using the average size and standard deviation is presented in Fig. 14.

FTIR analysis

FTIR spectra of the TIO_2 nanoparticles produced at the different stirring time of (a) 20 min (b) 40 min (c) 60 min (d) 80 min and (e) 100 min are shown in Fig. 15. The absorption band at 1639.54 cm^{-1} for TiO_2 produced at stirring time of 40, 60 80 and 100 min is assigned to H–O–H bending. At the stirring time of 60 min, it was noted that the intensity of bands between 535 and 600 cm^{-1} decreased. A strong absorption peak appeared in the TiO_2 nanoparticles produced at stirring time of 20, 40, 80 and 100 min and was associated with the vibrational modes of Ti–O–Ti bonds [58]. This is an indication that the intensities of the bands promote the Ti–O network resulting in the formation of TiO_2 nanoparticles (Fig. 16). In the cases of the FTIR spectra of TiO_2 nanoparticles produced at different pH (a) 2 (b) 4 (c) 6 (d) 8 (e) 10 and (f) 12 calcined shown in Fig. 16, absorption peaks in the range 520–630 cm^{-1}, assigned to Ti–O stretching modes was observed [29]. This particular absorption band also corresponds to tetrahedral $[TiO4]^{4-}$ units. At a pH of 8, a broader band observed at 630 cm^{-1} was linked to O-Ti–O and Ti–O-Ti of the TiO_2 framework. The formation of the anatase phase of TiO_2 at basic medium has the tendency of the bond breakage of Ti–O-Ti by NaOH to Ti–O-Na, suggesting the presence of high concentration of NaOH during the synthesis could influence the crystal growth of sodium titanate ($Na_2Ti_3O_7$).

XPS analysis

Figures 17, 18, 19 represent the general survey and the deconvoluted XPS spectra of TiO_2 nanoparticles synthesized by sol–gel method. Figure 17 shows the general XPS survey of Ti in the nanoparticle shows strong signals of Ti LMM, O KLL, O (1 s), Ti (2 s), C (1 s), Ti (2p), Ti (3 s) and Ti (3p) at different binding energies. While Fig. 18 which show the deconvoluted XPS spectra of Ti 2p revealed the presence of Ti ($2p_{1/2}$) and Ti ($2p_{3/2}$) corresponds to the atomic percentage of 32.8 and 67.2%, respectively. This indicates that Ti exists in the + 4 oxidation state and was obtained from the spin–orbit splitting of Ti ($2p_{1/2}$) and Ti ($2p_{3/2}$) electron bands. The energy difference between the doublets peaks is approximately 6 eV, thus confirmed the presence of Ti in + 4 and oxidation, not + 3 (Fig. 18). The existence of Ti in the chemical valence state of + 4 corroborated the previous studies [59]. The Ti LMM Auger transition exhibits a sharp peak in the region 880 eV, which corroborated to the crystal TiO_2.

These two identified peaks at 464.9 eV (Ti $2p_{1/2}$) and 458.8 eV (Ti $2p_{3/2}$) in Fig. 18 are similar to the published work reported by Krishnan et al. [60] who found that peaks for Ti^{4+} located at 459.3 and 465 eV, respectively. The two major peaks in O (1 s) in Fig. 19 lie between the binding energy of 529.5 eV and 530.9 eV. The hump shape of the O 1 s spectrum shows the presence of embedded surface species which were ascribed to four peaks at 530.7, 531.9, 532.9 and 534 eV as represented in Fig. 19. The initial peak at 530.7 eV represents the lattice O band to Ti^{4+} and the other three peaks emanated from water molecules on the surface of the sample. The order of OH group with oxygen can be found at the bridging oxygen site (531.9 eV), as a terminal group while oxygen attached to the five coordinated Ti^{4+} (O-Ti^{4+}) covalent bond existed at a binding energy of 533 eV and formation of a water molecule was confirmed with the binding energy of 534 eV.

Conclusion

In summary, TiO_2 nanoparticles were synthesized by sol–gel method and the effects of stirring time and solution pH were investigated. The prepared TiO_2 nanoparticles were characterized by different analytical tools. The characterization tools confirmed the successful synthesis of TiO_2 nanoparticles via sol–gel method. The optimum conditions to prepare well-distinct and evenly distributed spherical TiO_2 nanoparticles of tetragonal anatase phase were: solution pH (8) and stirring time (80 min), respectively. It was found that the stirring time and pH significantly influenced only the crystallite sizes and not the phase types of TiO_2 nanoparticles. The crystallite size obtained from W–H analysis shows variation which could be as a result of the difference in average the particle size distribution. It was revealed that W–H crystallite sizes at the acidic and basic media were significantly different from the size obtained using the Debye–Scherrer equation. The HRTEM images of TiO_2 illustrated that the inter-planar distances for SAED ring patterns were in agreement with the XRD plane results. The XPS analysis demonstrated two peaks located at the binding energies of 464.9 eV (Ti $2P_{1/2}$) and 458.8 eV (Ti $2P_{3/2}$).

Funding This study was funded by the Tertiary Education Trust Fund (TETFund) of Nigeria under a grant number TETFUND/FUTMINNA/2017/01.

Declarations

Conflict of interest Authors have declared that there is no conflict of interest.

References

1. Ansari, F., Soofivand, F., Salavati-Niasari, M.: Utilizing maleic acid as a novel fuel for synthesis of $PbFe_{12}O_{19}$ nanoceramics via sol–gel auto-combustion route. Mater. Charact. **103**, 11 (2015)
2. Sabry, R.S., Al-Haidarie, Y.K., Kudhier, M.A.: Synthesis and photocatalytic activity of TiO_2 nanoparticles prepared by sol-gel method. J. Sol-Gel Sci. Technol **78**(2), 299 (2016)
3. Haider, A.J., Al-Anbari, R.H., Kadhim, G.R., Salame, C.T.: Exploring potential environmental application of TiO_2 nanoparticles. Energy Procedia **119**, 332–345 (2017)
4. Tijani, J.O., Fatoba, O.O., Totito, T.C., Roos, W.D., Petrik, L.F.: Synthesis and characterization of carbon doped TiO_2 photocatalysts supported on stainless steel mesh by sol-gel method. Carbon Lett. **22**, 48 (2017)
5. Ebrahimi, H.R., Parish, M., Amiri, G.R., Bahraminejad, B., Fatahian, S.: Synthesis, characterization and gas sensitivity investigation of NiO.5ZnO. $5Fe_2O_4$ nanoparticles. J. Mag. Mag. Mater **414**, 55–58 (2016)
6. Ebrahimi, H.R., Usefi, H., Emami, H., Amiri, G.R.: Synthesis, characterization, and sensing performance investigation of copper cadmium ferrite nanoparticles. IEEE Trans. Magn. **54**(10), 1–5 (2018)
7. Budarz, J.F., Cooper, E.M., Gardner, C., Hodzic, E., Ferguson, P.L., Gunsch, C.K., Wiesner, M.R.: Chlorpyrifos degradation via photoreactive TiO_2 nanoparticles: assessing the impact of a multi-component degradation scenario. J. Hazard. Mater. **372**, 61–68 (2019)
8. Eskandari, Z., Talaiekhozani, A., Talaie, M.R., Banisharif, F.: Enhancing ferrate (VI) oxidation process to remove blue 203 from wastewater utilizing MgO nanoparticles. J. Environ. Manag. **231**, 297–307 (2019)
9. Li, B., Zhang, X., Dou, J., Hu, C.: Facile synthesis of pseudocapacitive Mn_3O_4 nanoparticles for high-performance supercapacitor. Ceram. Inter **45**(13), 16297–16304 (2019)
10. Ebrahimi, H.R., Modrek, M., Joohari, S.: Photodecolorization of direct yellow 86 (2- Solamine) by using zinc oxide nanosized deposited on glass beads. Indian J. Sci. Technol. **5**(1), 1828–1830 (2012)

11. Ebrahimi, H.R., Modrek, M.: Photocatalytic decomposition of methyl red dye by using nanosized zinc oxide deposited on glass beads in various pH and various atmosphere. J. Chem. **2013**, 1–4 (2013)
12. Ghowsi, K., Ebrahimi, H.R., Kazemipour-Baravati, F., Bagheri, H.: Synthesize of ZnO/NPs and investigation of its effect in reduction of electrochemical charge transfer resistance; application of it for photodecomposition of calcon (CI 15705) dye in various media. Inter J. Electrochem. Sci. **9**(4), 1738–1746 (2014)
13. Ebrahimi, H.R., Modrek, M., Joohari, S.: Photodegradation of methyl orange dye by using zinc oxide nano-sized catalysts on glass granules at various ph values and different atmosphere. Fresenius Environ. Bull. **23**(5), 1155–1158 (2014)
14. Zhong, W., Tu, W., Feng, S., Xu, A.: Photocatalytic H_2 evolution on CdS nanoparticles by loading FeSe nanorods as co-catalyst under visible light irradiation. J. Alloys Compd. **772**, 669–674 (2019)
15. Gopala, K.V., Purushothaman, A., Elango, P.: A study of the physical properties and gas-sensing performance of TiO_2 nanofilms: Automated nebulizer spray pyrolysis method (ANSP). Phys. Status Solidi **214**(10), 1–9 (2017)
16. Rao, B.G., Mukherjee, D., Reddy, B.M.: Novel approaches for the preparation of nanoparticles. In: Nanostructures for Novel Therapy, Synthesis Characterization and Applications. Micro and Nano Technology, pp. 1–36. Elsevier, Amsterdam (2017)
17. Sofyan, N., Ridhova, A., Yuwono, A.H., Udhiarto, A.: Preparation of anatase TiO_2 nanoparticles using low hydrothermal temperature for dye-sensitized solar cell. IOP Conf. Ser. Mater. Sci. Eng. **316**, 0120551 (2018)
18. Yudoyono, G., Ichzan, N., Zharvan, V., Daniyati, R., Santoso, H., Indarto, B., Pramono, Y.H., Zainuri, M., Darminto, H.: Effect of calcination temperature on the photocatalytic activity of TiO_2 powders prepared by co-precipitation of TiCl3. AIP Conf. Proc. **1725**, 1–7 (2020)
19. De Filpo, G., Pantuso, E., Armentano, K., Formoso, P., Di Profio, G., Poerio, T., Fontananova Meringolo, E.C., Mashin, A.I., Nicoletta, F.P.: Chemical vapor deposition of photocatalyst nanoparticles on PVDF membranes for advanced oxidation processes. Membranes **8**, 35 (2018)
20. Aziz, W.J., Ali, S.Q., Jassim, N.Z.: Production TiO_2 nanoparticles using laser ablation in ethanol. SILICON **10**(5), 2101–2107 (2018)
21. Torabmostaedi, H., Zhang, T.: Numerical simulation of TiO_2 nanoparticle synthesis by flame spray pyrolysis. Powder Technol. **329**, 426–433 (2018)
22. Aramwit, C., Yu, L.D., Gregoratti, L., Choopons, S.: Characterizations and DSSC efficiency test of TiO_2 nano-films formed by filtered cathodic vacuum arc deposition. Int. J. Nanotechnol. **14**(1), 481–495 (2017)
23. Kang, O.L., Ahmad, A., Rana, U.A., Hassan, N.H.: Sol-gel titanium dioxide nanoparticles: Preparation and structural characterization. J. Nanotechnol. (2016). https://doi.org/10.1155/2016/5375939
24. Nateq, M.H., Ceccato, R.: Sol-gel synthesis of TiO_2 nanocrystalline particles with enhanced surface area through the reverse micelle approach. Adv. Mater. Sci. Eng. **12**(11), 1744 (2019)
25. Selman, A.M., Hassan, Z., Husham, Z.: Structural and photoluminescence studies of rutile TiO_2 nanorods prepared by chemical bath deposition method on Si substrates at different pH values. Measurement **56**, 155–162 (2014)
26. Xue, J., Shen, Q., Yang, F., Liang, W., Liu, X.: Investigation on the influence of pH on the structure and photoelectrochemical properties of CdSe electrolytically deposited into TiO_2 nanotube arrays. J. Alloys Compd. **607**, 163–168 (2014)
27. Mohite, V.S., Mahadik, M.A., Kumbhar, S.S., Kothavale, V.P., Moholkar, A.V., Rajpure, K.Y., Bhosale, C.H.: Photo-electrocatalytic degradation of benzoic acid using sprayed TiO_2 thin films. Ceram. Int. **41**, 2202–2208 (2015)
28. Tsega, M., Dejene, F.B.: Influence of acidic pH on the formulation of TiO_2 nanocrystalline powders with enhanced photoluminescence property. Heliyon **3**, 1–16 (2017)
29. Shehap, A.M., Akil, D.S.: Structural and optical properties of TiO2 nanoparticles/PVA for different composites thin films. Inter. J. Nanoelectron. Mater. **9**, 17–36 (2016)
30. Priyanka, K.P., Sheena, P.A., Sabu, N.A., George, T., Balakrishna, K.M., Varghese, T.: Characterization of nanophase TiO_2 synthesized by sol-gel method. Indian J. Phys. **88**(7), 657–663 (2014)
31. Kibasomba, P.M., Dhlamini, S., Maaza, M., Liu, C.P., Rashad, M.M., Rayan, D.A., Mwakikunga, B.W.: Strain and grain size of TiO_2 nanoparticles from TEM, Raman spectroscopy and XRD: The revisiting of the Williamson-Hall plot method. Results Phys. **9**, 628–635 (2018)
32. Singh, P.K., Mukherjee, S., Ghosh, C.K., Maitra, S.: Influence of precursor type on structural, morphological, dielectric and magnetic properties of TiO_2 nanoparticles. Cerâmica **63**, 549–556 (2017)
33. Singh, P.K., Mukherjee, S., Ghosh, C.K., Maitra, S.: Spectroscopic investigation on sol gel derived TiO_2 nanoparticles. J. Adv. Nanomater. **2**(3), 160–168 (2017)
34. Fu, R., Yin, Q., Guo, X., Tong, X., Wang, X.: Evolution of mesoporous TiO_2 during fast sol-gel synthesis. Res. Chem. Intermed. **43**(11), 6433–6445 (2017)
35. Morales, J., Maldonado, A., de La, M., Olvera. L.: 10th International Conference on Electrical Engineering, Computing Science and Automatic Control (CCE) Mexico City, Mexico (2013)
36. Islam, S.Z., Nagpure, S., Kim, D.Y., Rankin, S.E.: Synthesis and catalytic applications of non-metal doped mesoporous titania. Inorganics **5**(15), 1–43 (2017)
37. Pavel, K., Radovan, K.: The effect of calcination on the structure of inorganic tio$_2$ nanofiber, Oct 14th–16th 2015, Brno, Czech Republic, EU. NanoCon (2015)
38. El-Mekkawi, D.M., Labib, A.A., Mousa, H.A., Galal, H.R., Mohamed, W.A.: A preparation and characterization of nano titanium dioxide photocatalysts via sol-gel method over narrow ranges of varying parameters. Orient. J. Chem. **33**(1), 41–51 (2017)
39. Kumar, S.G., Rao, K.K.: Polymorphic phase transition among the titania crystal structures using a solution-based approach: from precursor chemistry to nucleation process. Nanoscale **6**(20), 11574–11632 (2014)
40. Mirjalili, F., Manafi, S., Farahbakhsh, I.: Preparation and characterization of TiO_2 nanoparticles prepared by sol-gel method. Adv. Ceram. Prog. **3**(3), 38–47 (2017)
41. Hajjaji, W., Andrejkovičová, S., Pullar, R.C., Tobaldi, D.M., Lopez-galindo, A., Jammousi, F., Rocha, F., Labrincha, J.A.: Effective removal of anionic and cationic dyes by kaolinite and TiO_2/kaolinite composites. Clay Miner. **51**, 19–27 (2016)
42. Nyamukamba, P., Okoh, O., Mungondori, H., Taziwa, R., Zinya, S.: Synthetic methods for titanium dioxide nanoparticles: a review. In: Yang, D. (ed.) Titanium Dioxide-Material for a Sustainable Environment, pp. 151–1755. InTech, London (2018)
43. Victoria, D.B., Hernández, P.I., Garibay, F.V., Díaz, B.A.L., Suárez, P.R., Rivera, O.J.N., Luna, P.R., Melo, M.D.V., González, R.L.: Atomic-scale investigation on the evolution of Tio$_2$-anatase prepared by a sonochemical route and treated with NaOH. Materials **13**(3), 685 (2020)
44. Bitaraf, M., Ghazi, M.E., Izadifard, M.: Studying structural and optical properties of TiO_2-SnO_2 core-shell synthesized by sol-gel route. Cryst. Res. Technol. **55**(3), 1900145 (2020)

45. El-Nagar, H., Abd El-sadek, M.S., Ezzeldien, M.: Structural analysis, optical and mechanical properties of $Ti_xZr_{1-x}O_2$ nanoparticles synthesized by modified co-precipitation route. Appl. Phys. A **126**(2), 126 (2020)
46. Raguram, T., Rajni, K.S.: Effects of varying the soaking duration of Eosin Blue sensitized TiO_2 photoanodes for dye-sensitized solar cells. Optik **204**, 164169 (2020)
47. Rajan, M.T., Hassan, E.: Laser plasma induced TiO_2 nanoparticle synthesis in water and particle characterization. IEEE Access **7**, 56556–56563 (2019)
48. Gao, Z., Wu, Z., Chen, X., Yang, X.: Effective synthesis of nanoscale anatase TiO_2 single crystals using activated carbon template to enhance the photodegradation of crystal violet. Appl. Organomet. Chem. **33**(3), e4664 (2019)
49. Ibrahim, I., Kaltzoglou, A., Athanasekou, C., Katsaros, F., Devlin, E., Kontos, A.G., Ioannidis, N., Perraki, M., Tsakiridis, P., Sygellou, L., Antoniadou, M.: Magnetically separable $TiO_2/CoFe_2O_4$/Ag nanocomposites for the photocatalytic reduction of hexavalent chromium pollutant under UV and artificial solar light. Chem. Eng. J. **381**, 122730 (2020)
50. Komaraiah, D., Radha, E., Kalarikkal, N., Sivakumar, J., Reddy, M.R., Sayanna, R.: Structural, optical and photoluminescence studies of sol-gel synthesized pure and iron doped TiO_2 photocatalysts. Ceram. Inter. **45**(18), 25060–25068 (2019)
51. Nabi, G., Raza, W., Tahir, M.B.: Green synthesis of TiO_2 nanoparticle using cinnamon powder extract and the study of optical properties. J Inorg. Organomet. Polym. Mater. **30**, 1425 (2020)
52. Ndabankulu, V.O., Maddila, S., Jonnalagadda, S.B.: Synthesis of lanthanide-doped TiO_2 nanoparticles and their photocatalytic activity under visible light. Canad. J. Chem. **97**(9), 672–681 (2019)
53. Azizi-Lalabadi, M., Ehsani, A., Divband, B., Alizadeh-Sani, M.: Antimicrobial activity of Titanium dioxide and Zinc oxide nanoparticles supported in 4A zeolite and evaluation the morphological characteristic. Sci. Rep. **9**(1), 1–10 (2019)
54. Siliveri, S., Chirra, S., Tyagi, C., Gandamalla, A., Adepu, A.K., Goskula, S., Gujjula, S.R., Venkatathri, N.: New porous high surface area, TiO_2 Anatase/SAPO-35 mild brønsted acidic nanocomposite: Synthesis, characterization and studies on it's enhanced photocatalytic activity. ChemistrySelect **4**(31), 9135–9142 (2019)
55. Venkatachalam, P., Kalaivani, T., Krishnakumar, N.: Erbium doped anatase TiO_2 nanoparticles for photovoltaic applications. Opt. Quantum Electron. **51**(9), 315 (2019)
56. Wu, Y., Fu, Y., Zhang, L., Ren, Y., Chen, X., Yue, B., He, H.: Study of oxygen vacancies on different facets of anatase TiO_2. Chin. J. Chem. **37**(9), 922–928 (2019)
57. Soni, H., Kumar, J.N., Patel, K., Kumar, R.N.: Photocatalytic decoloration of three commercial dyes in aqueous phase and industrial effluents using TiO_2 nanoparticles. Des. Water Treat. **57**(14), 6355–6364 (2016)
58. León, A., Reuquen, P., Garín, C., Segura, R., Vargas, P., Zapata, P., Orihuela, P.: A FTIR and Raman characterization of TiO_2 nanoparticles coated with polyethylene glycol as carrier for 2-methoxyestradiol. Appl. Sci. **7**(1), 49 (2017)
59. Liu, X., Xu, L., Huang, Y., Qin, C., Qin, L., Seo, H.J.: Improved photochemical properties of Aurivillius $Bi_5Ti_3FeO_{15}$ with partial substitution of Ti^{4+} with Fe^{3+}. Ceram. Inter. **43**(15), 1237–1238 (2017)
60. Krishnan, P., Liu, M., Itty, P.A., Liu, Z., Rheinheimer, V., Zhang, M.H., Monteiro, P.J.M., Yu, L.E.: Characterization of photocatalytic TiO_2 powder under varied environments using near ambient pressure X-ray photoelectron spectroscopy. Sci. Rep. **7**(1), 1 (2017)